frontiers | Frontiers in Physics

TYPE Original Research
PUBLISHED 18 July 2024
DOI 10.3389/fphy.2024.1420138

OPEN ACCESS

EDITED BY
Heloisa N. Bordallo,
University of Copenhagen, Denmark

REVIEWED BY
Perviz Sayan,
Marmara University, Türkiye
Rodrigo Lima,
University of Copenhagen, Denmark
Francisco Sousa,
Federal University of Pará, Brazil

*CORRESPONDENCE
Su-hong Yin,
shyinjob@163.com

RECEIVED 19 April 2024
ACCEPTED 25 June 2024
PUBLISHED 18 July 2024

CITATION
Li G-g, Liu J-e, Ma L, Gong H-l and Yin S-h (2024), Impact of carboxylic acid structure on α-hemihydrate gypsum crystal morphology and mechanical strength.
Front. Phys. 12:1420138.
doi: 10.3389/fphy.2024.1420138

Impact of carboxylic acid structure on α-hemihydrate gypsum crystal morphology and mechanical strength

Guo-gang Li[1,2,3], Jin-e Liu[2], Liang Ma[4], Hao-lei Gong[5] and Su-hong Yin[1]*

[1]College of Materials Science and Engineering, South China University of Technology, Guangzhou, China, [2]Hubei Yuangu New Building Materials Technology Co., Ltd, Yichang, China, [3]Yichang Building Energy Conservation Promotion Center, Yichang, China, [4]Guangdong Provincial Transportation Construction Engineering Quality Affairs Center, Guangzhou, China, [5]Three Gorges Public Inspection and Testing Center, Yichang, China

This study investigated the synthesis of α-hemihydrate gypsum (α-HH) through semi-liquid autoclaving of phosphogypsum (PG) using various carboxylic acids as modifying agents. The impact of carboxyl group spatial location, auxiliary functional group type, and the number of carboxyl groups within the carboxylic acid modifiers on the mechanical strength and crystal morphology of α-HH was analyzed using scanning electron microscopy (SEM), strength testing, and molecular dynamics simulations. The results revealed a significant influence of the carboxylic acid molecular structure on the α-HH crystal morphology. Monocarboxylic acids and dicarboxylic acids with a long carbon chain length between carboxyl groups exhibited preferential adsorption on the (200), (110), and (–110) crystal planes, promoting crystal growth along the c-axis. In contrast, hydroxyl groups and cis double bonds in the modifier structure induced selective adsorption on the (001) plane, hindering growth along the c-axis. Conversely, trans double bonds favored adsorption on the (200), (110), and (–110) planes, enhancing growth along the c-axis. Based on these observations, screening principles for carboxylic acid modifiers were established, suggesting that: 1) the number of carboxyl groups should exceed 2; 2) the optimal carbon atom spacing between carboxyl groups is 3; and 3) auxiliary functional groups such as hydroxyl groups and cis double bonds should be introduced. Modifiers like citric acid, ethylene diamine tetraacetic acid (EDTA), and pyromellitic acid, within concentration ranges of 0.05%–0.1%, 0.1%–0.15%, and 0.05%–0.1%, respectively, yielded α-HH with flexural strengths exceeding 4 MPa and compressive strengths greater than 35 MPa, demonstrating the validity of these principles.

KEYWORDS

α-hemihydrate gypsum, carboxylic acid modifiers, phosphogypsum, semi-liquid autoclaving, molecular dynamics simulation

1 Introduction

Phosphogypsum (PG), a major by-product of wet-process phosphoric acid production, poses a significant environmental challenge. Global PG production is estimated at approximately 5 tons per ton of phosphoric acid [1], resulting in massive accumulations, particularly in China, where over 830 million tons are stockpiled, with

an annual increase of 78 million tons [2, 3]. This large-scale accumulation not only occupies valuable land and contaminates the environment [4–6] but also poses potential safety risks. Consequently, comprehensive and sustainable utilization of PG is crucial, focusing on high-value applications and large-scale technological pathways.

Current PG utilization technologies, despite their diversity, face limitations. Utilizing PG in cement retarders, phosphor gypsum-based composites [7–10], and β-hemihydrate gypsum often suffers from low added value and restricted application domains [11–14]. For instance, phosphor gypsum matrix composite cements exhibit low alkalinity and susceptibility to carbonation, limiting their use to plain concrete applications. While β-hemihydrate gypsum is suitable for lower-end products, it exhibits high water consumption and low strength properties. Utilizing PG for road construction [15–17] and mine filling offers minimal added value with uncertain environmental impacts [18].

A promising alternative is the transformation of PG into α-hemihydrate gypsum (α-HH) through dehydration via heating in saturated steam or aqueous solutions [19–21]. α-HH is a valuable resource with applications in gypsum-based self-leveling mortars, mold gypsum, and fiber-reinforced gypsum boards, among others. However, the fibrous morphology of α-HH crystals, due to their preferential growth along the c-axis direction, compromises their mechanical properties. To overcome this limitation, controlling the growth habit and morphology of α-HH crystals is crucial. This can be achieved by transforming them into short columnar forms through the use of crystal modifiers. Crystal modifiers selectively adsorb onto different crystal planes of α-HH crystals, altering the surface energy ratio and influencing crystal plane growth rates, thus modifying the overall crystal morphology [22–24].

While three types of modifiers are currently utilized (inorganic salts, low-polymerization organic acids, and high-polymerization organic acid surfactants), each presents drawbacks. Inorganic salts, such as aluminum sulfate, magnesium sulfate, and sodium sulfate, may lead to salt petering on the product surface due to their high content. High-polymerization organic acid surfactants, commonly used for preparing calcium sulfate whiskers, promote growth along the c-axis, increasing the aspect ratio. Carboxylic acids, however, have proven to be well-suited for producing α-HHs due to their ability to selectively adsorb onto end surfaces of α-HH crystals, retarding their growth rate along the c-axis direction [25–30].

Current research on carboxylic acid modifiers primarily focuses on investigating the impact of different carboxylic modifiers and quantities on the morphology and performance of α-HH [31–34]. However, understanding how the molecular structure of carboxylic acids themselves influences the performance and crystal morphology of α-HH, along with its underlying mechanism, remains an important area of research. Carboxylic acids, besides their carboxyl functional group, may contain auxiliary functional groups like hydroxyl or carbon-carbon double bonds, with variations in both number and spatial position. Establishing a screening principle for carboxylic acid modifiers based on their molecular structure is crucial for optimizing α-HH production.

This study investigates the effects of carboxylic acids with diverse molecular structures on the mechanical strength and crystal morphology of α-HH. Experiments were conducted using citric acid, ethylene diamine tetraacetic acid (EDTA), and pyromellitic acid as modifiers, guided by screening principles established through molecular dynamics simulations. These simulations calculated the adsorption energy of various carboxylic acids on different crystal planes of α-HH, offering insights into how molecular structure influences α-HH crystal growth. This combined experimental and computational approach provides a comprehensive understanding of the relationship between carboxylic acid molecular structure and α-HH crystal morphology, paving the way for the development of effective and targeted strategies for α-HH production.

2 Experiment

2.1 Materials and pretreatment

The original phosphogypsum (PG) used in this study was obtained from Hubei Yuangu Group. To remove harmful impurities, the original PG underwent pretreatment with alkaline hot water at 70°C and pH = 12 washing. The process involved a mass ratio of alkaline hot water to PG of 1:1, with PG being washed once, followed by drying in an oven at 55°C ± 5°C until completely dry. Subsequently, the PG was sieved through a 0.3 mm square-hole mesh. The chemical composition of PG samples was analyzed by X-ray fluorescence spectrometer (Axios PW4400). The results are shown in Table 1. The crystalline phases and morphology of PG samples were analyzed respectively by X-ray diffraction (XRD-6000, Shimadzu, Japan) and scanning electron microscopy (Zeiss EV018). The results are shown in Figures 1, 2, respectively. The main components of the original PG were $CaSO_4{\cdot}2H_2O$ and SiO_2, along with trace amounts of alkaline earth metal oxides and P_2O_5. The crystal morphology of PG presents as rhomboidal-like particles. After pretreatment, the impurities were significantly reduced and $CaSO_4{\cdot}2H_2O$ content increased. The pretreatment did not alter the crystal morphology of PG, but significantly reduced the presence of fine particles adhering to the surface of the crystals.

All modifiers used were analytical reagents which degree of purity were greater than 99%, sourced from Shanghai Maclin Biochemical Technology Company. These included formic acid, adipic acid, maleic acid, succinic acid, glutaric acid, dodecanedioic acid, mannitic acid, ethylene diamine tetraacetic acid (EDTA), 2-hydroxy succinic acid, maleic acid, reverse succinic acid, citric acid, and pyromellitic acid.

2.2 Preparation of α-HH sample

Formic acid, adipic acid, maleic acid, succinic acid, glutaric acid, dodecanedioic acid, mannitic acid, 2-hydroxy succinic acid, maleic acid, and reverse succinic acid were separately dissolved in deionized water at a concentration of 0.05% by weight of PG. Citric acid, EDTA, and pyromellitic acid were dissolved separately in deionized water at concentrations of 0.05%, 0.1%, 0.15%, and 0.2% by weight of PG.

Subsequently, the water was thoroughly mixed with the pretreated PG using a mixer to prepare the slurry, with a mass ratio of 0.3 of water to PG. The slurry was then autoclaved at 140°C ± 5°C for 3 h. The resulting α-HH was dried at 140°C ± 5°C for 12 h, followed by 20 min of grinding. Finally, it was sieved through a 0.125 mm square-hole mesh.

10.3389/fphy.2024.1420138

TABLE 1 Chemical composition of original PG and purified PG (wt%).

	F	NaO	MgO	Al_2O_3	SiO_2	P_2O_5	SO_3	K_2O	CaO	TiO_2	Fe_2O_3
Original PG (O-PG)	1.56	0.46	0.25	0.42	6.80	1.03	49.0	0.18	39.80	0.10	0.30
Purified PG (P-PG)	1.27	0.52	0.08	0.11	5.81	0.79	49.5	0.09	41.03	0.12	0.27

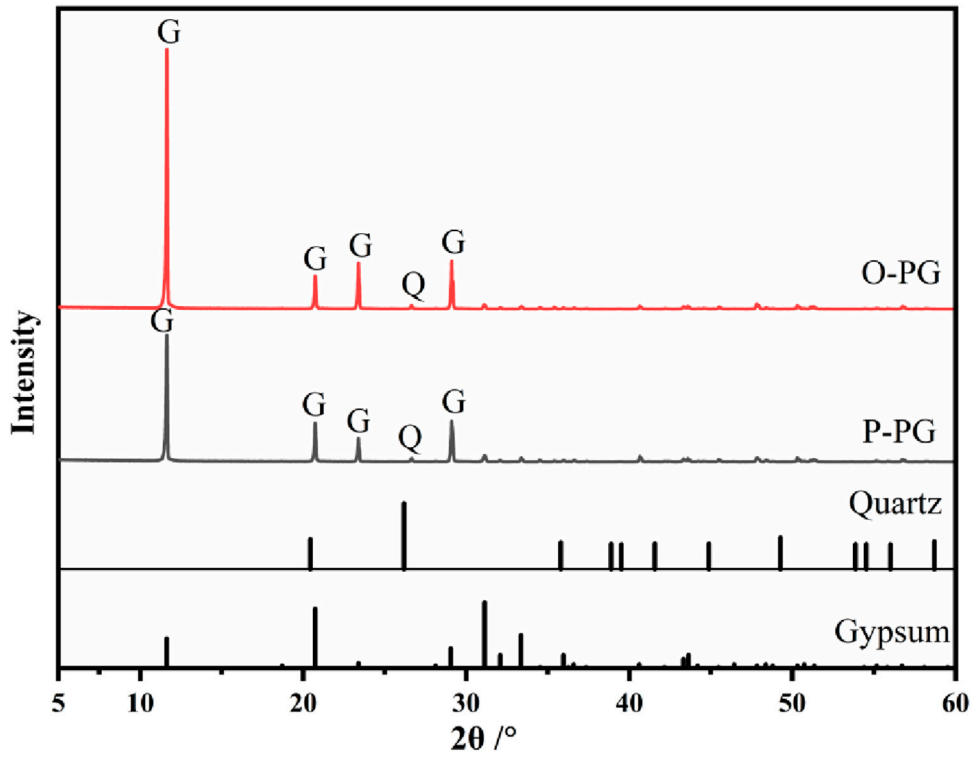

FIGURE 1
XRD patterns of PG. (G-gypsum, Q-quartz).

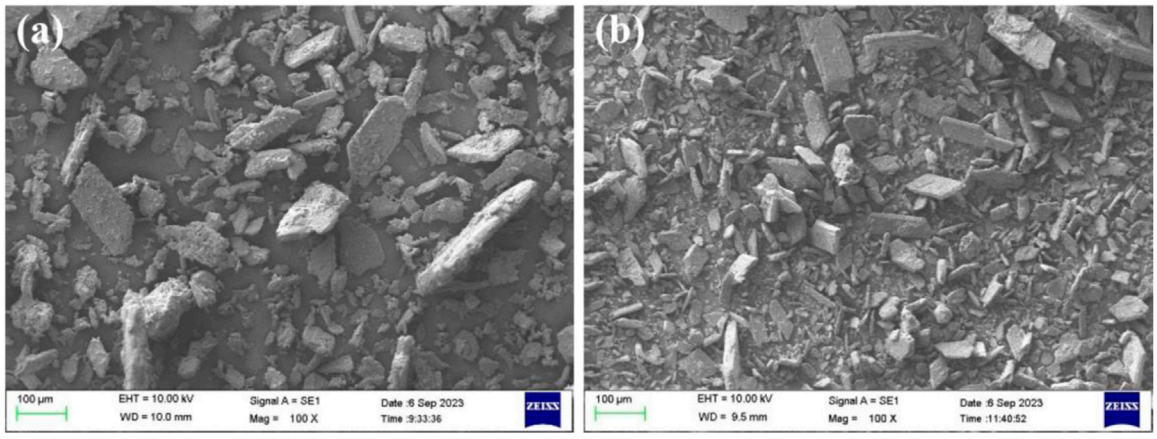

FIGURE 2
SEM images of PG: **(A)** original PG, **(B)** purified PG.

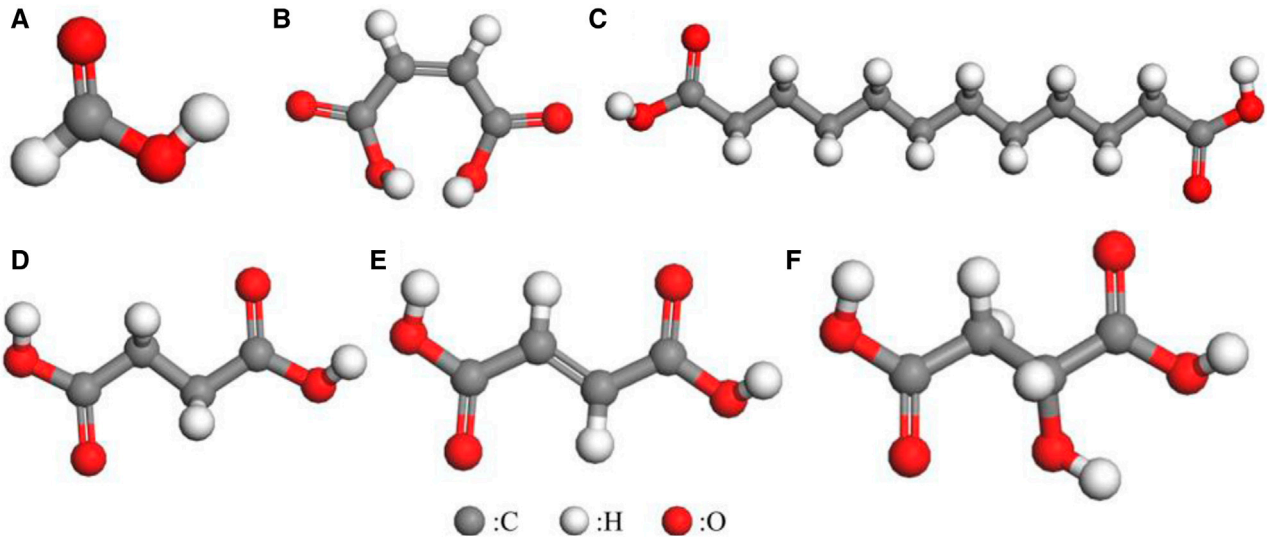

FIGURE 3
Molecular models of different carboxylic modifiers:**(A)** formic acid, **(B)** maleic acid, **(C)** dodecanedioic acid, **(D)** succinic acid, **(E)** reverse succinic aid, **(F)** 2-hydroxy succinic aid.

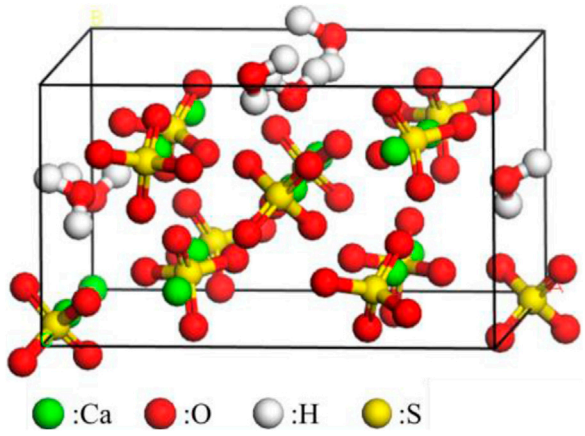

FIGURE 4
$CaSO_4{\cdot}0.5H_2O$ crystal cell model obtained through molecular dynamics simulations.

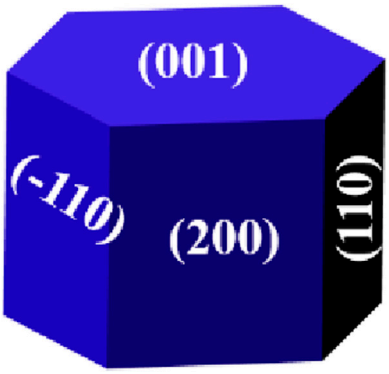

FIGURE 5
Morphology of α-HH crystals predicted by BFDH theory.

2.3 Methods

2.3.1 Mechanical strength test

A blade-type laboratory blender (NJ 160B, China) was used to prepare the α-HH slurry to standard consistency. The slurry was then cast into 40 mm × 40 mm × 160 mm molds and demolded after 2 h. Some specimens were tested for flexural strength after 2 h, while others were dried for 24 h at 40°C to assess dry compressive strength. Strength testing was conducted according to China Building Materials Industry Standard "Test methods for physical properties of ordinary gypsum plaster" (JC/T2038-2010) [35].

2.3.2 Microstructure

The sample phase composition was analyzed using an X-ray diffraction instrument, operating with Cu $K\alpha_1$ radiation (λ = 1.5418 Å) at a 40 kV voltage and 40 mA current. The angular testing range for 2θ is 5–60°.

The microstructure of the samples was observed using a Zeiss EV018 scanning electron microscope at a voltage of 10 kV and a current of 5 mA. Prior to testing, all specimens were coated with gold to ensure conductivity.

3 Molecular dynamics simulation of adsorption of modifier on the plane of α-HH crystals

3.1 Model construction and parameter settings

In this study, six different modifiers were selected, including formic acid (CH_2O_2), dodecanedioic acid ($C_{12}H_{22}O_4$), succinic

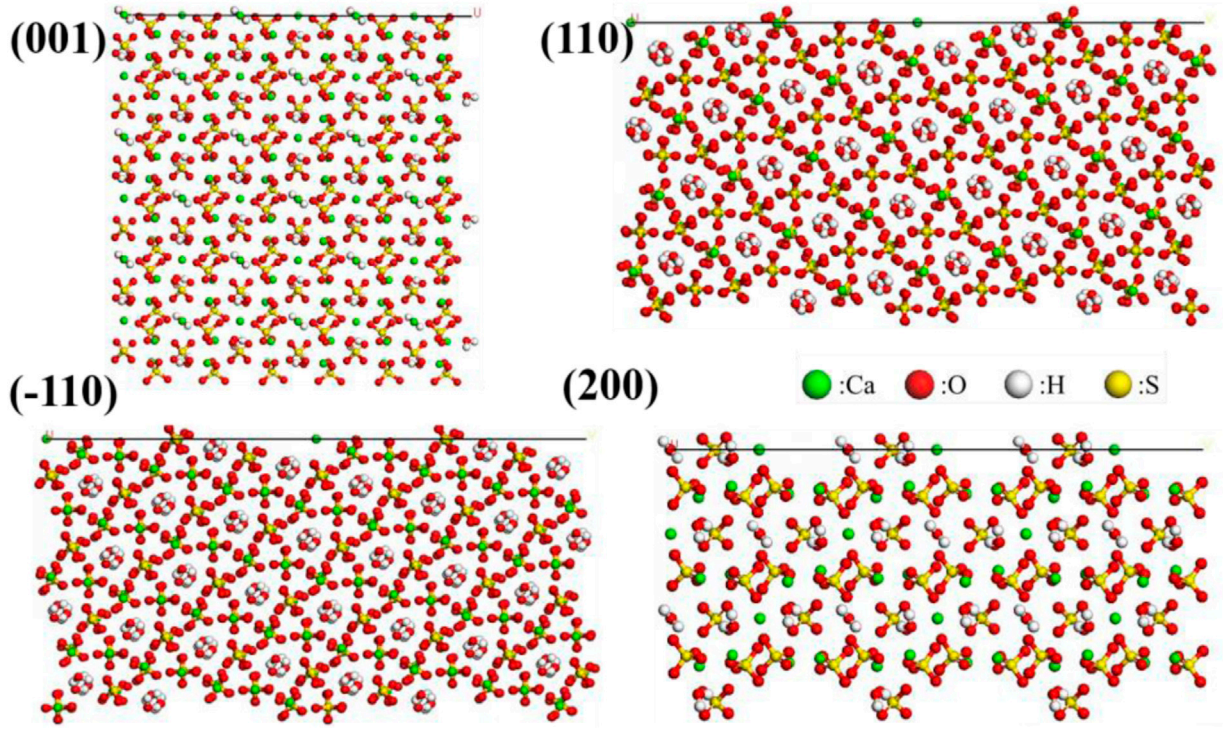

FIGURE 6
Structure models of the (001), (110), (−110), and (200) crystal planes of α-HH crystals obtained via molecular dynamics simulations.

acid ($C_4H_6O_4$),2-hydroxy succinic aid ($C_4H_6O_5$), reverse succinic aid ($C_4H_4O_4$), and maleic acid $C_4H_4O_4$). The molecular models of these modifiers are depicted in Figure 3. The cell model of $CaSO_4{\cdot}0.5H_2O$ crystal was constructed based on the literature [36], and the atomic coordinates of the crystal structure were exported from the CCDC database to establish the model, as illustrated in Figure 4. The lattice parameters are as follows: a = 12.0344 Å, b = 6.9294 Å, c = 90.265 Å, and β = 90.270°.

To describe the interaction between modifier molecules and different crystal planes of α-HH crystal, it is necessary to cleave several crystal planes of α-HH crystal. The predicted theoretical morphology of α-HH crystals, utilizing the Bravais-Friedel-Donnay-Harker (BFDH) theory, which is a model in crystallography that explains the growth and morphology of crystals, is illustrated in Figure 5 [37].

According to this theoretical morphology, the crystal planes (001), (−110), (200), and (110) of α-HH were selected as the adsorption crystal planes for the modifier. A 3 × 5 × 3 supercell structure of α-HH crystal was constructed, and models of the (001), (110), (−110), and (2 0 0) crystal planes were cleaved, as shown in Figure 6.

For the molecular models of modifiers and crystal planes, initial structures were geometrically optimized using the Forcite module with the Smart algorithm. The COMPASSII force field was employed for the molecular force field, and atomic charges were assigned using the Forcefield assigned method. A cutoff radius of 12.5 Å was applied. Van der Waals interactions were computed using the Atom-based method, while electrostatic interactions were calculated using the Ewald method.

The Adsorption Locator module in Materials Studio was utilized to perform a Monte Carlo search in the configuration space of the substrate-adsorbate system to determine potential low-energy adsorption configurations. The interface model was assembled by combining $CaSO_4{\cdot}0.5H_2O$ crystal planes with modifier molecules. The Simulated Annealing algorithm available in the Adsorption Locator module was employed to locate the adsorption points with the lowest potential energy. The COMPASSII force field was selected for the molecular force field, and atomic charges were assigned based on the COMPASSII force field. Atom-based method was used for van der Waals interactions, while electrostatic interactions were computed using the Group-based algorithm. The energy convergence criterion was set to 0.001 kcal/mol, and the cutoff radius was set to 12.5 ÅFigure 7 displays the adsorption models of formic acid on the (001), (110), (−110), and (200) crystal planes of α-HH crystals, while Figure 8 depicts the adsorption models of dodecanedioic acid on the (001), (110), (−110), and (200) crystal planes of α-HH crystals. Additionally, Figure 9 illustrates the adsorption models of succinic acid, 2-hydroxy succinic aid, reverse succinic aid and maleic acid on the (001) crystal plane of α-HH crystal.

3.2 Simulation of interaction energy

The stability of the adsorption system is indicated by the negative interaction energy between the modifier and various

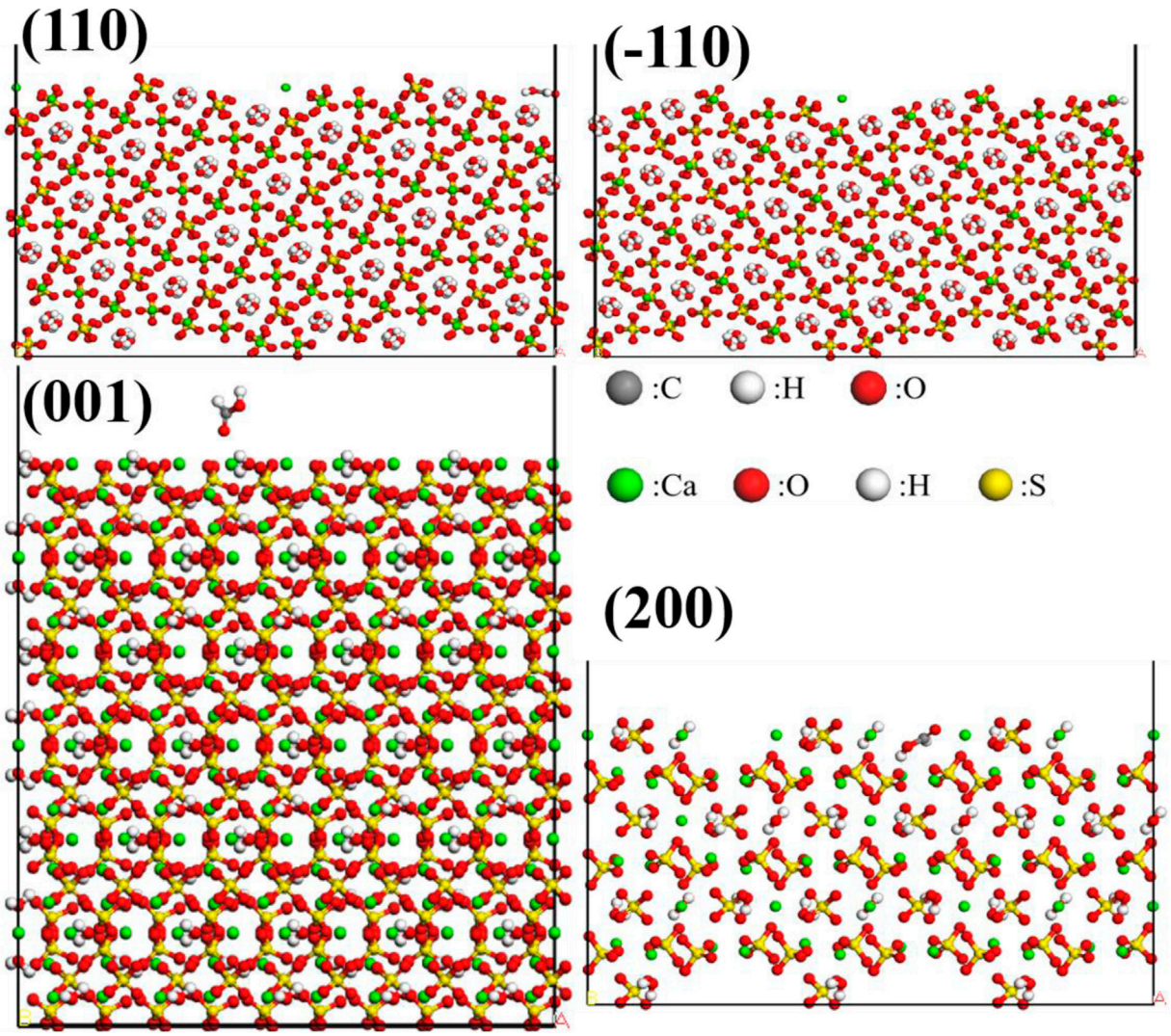

FIGURE 7
Adsorption models of formic acid on the (001), (110), (–110), and (200) crystal planes of α-HH crystals obtained via molecular dynamics simulations.

crystal surfaces of α-HH. A more negative interaction energy value indicates a more favorable and stable adsorption configuration [38]. To determine the position of the lowest energy structure when the modifier is absorbed on the crystal plane, we calculated the interaction energy between the modifier and different plane of the α-HH crystal.

The following Formula 1 was utilized to calculate the interaction energy between the modifier molecule and the crystal plane:

$$\Delta E = E_{total} - \left(E_{surface} + E_{modifier}\right) \quad (1)$$

In this equation, ΔE represents the interaction energy between the modifier molecule and the crystal plane; E_{total} represents the total energy of both the crystal plane and the modifier; $E_{surface}$ represents only the total energy of the crystal surface; and $E_{modifier}$ represents only the total energy of the modifier.

4 Results and discussion

4.1 Effect of molecular structure of carboxylic acids on the mechanical strength of α-HH

Figures 10, 11 depict the mechanical strength of α-HH samples prepared under the regulation of carboxylic acid modifiers with different molecular structures.

The mechanical strength of α-HH exhibited a non-monotonic trend with increasing carbon atom spacing between the carboxyl groups. Compared to the reference sample, α-HH showed a slight increase in mechanical strength when modified with carboxylic acids containing no intervening carbon atoms between the carboxyl groups. A more pronounced enhancement was observed with modifiers containing three carbon atoms within the carboxyl group interval. However, further increases in the number of separating carbon atoms led to a decline in mechanical strength. Notably, exceeding 10 spacer carbon atoms resulted in a reversal of the morphology control effect.

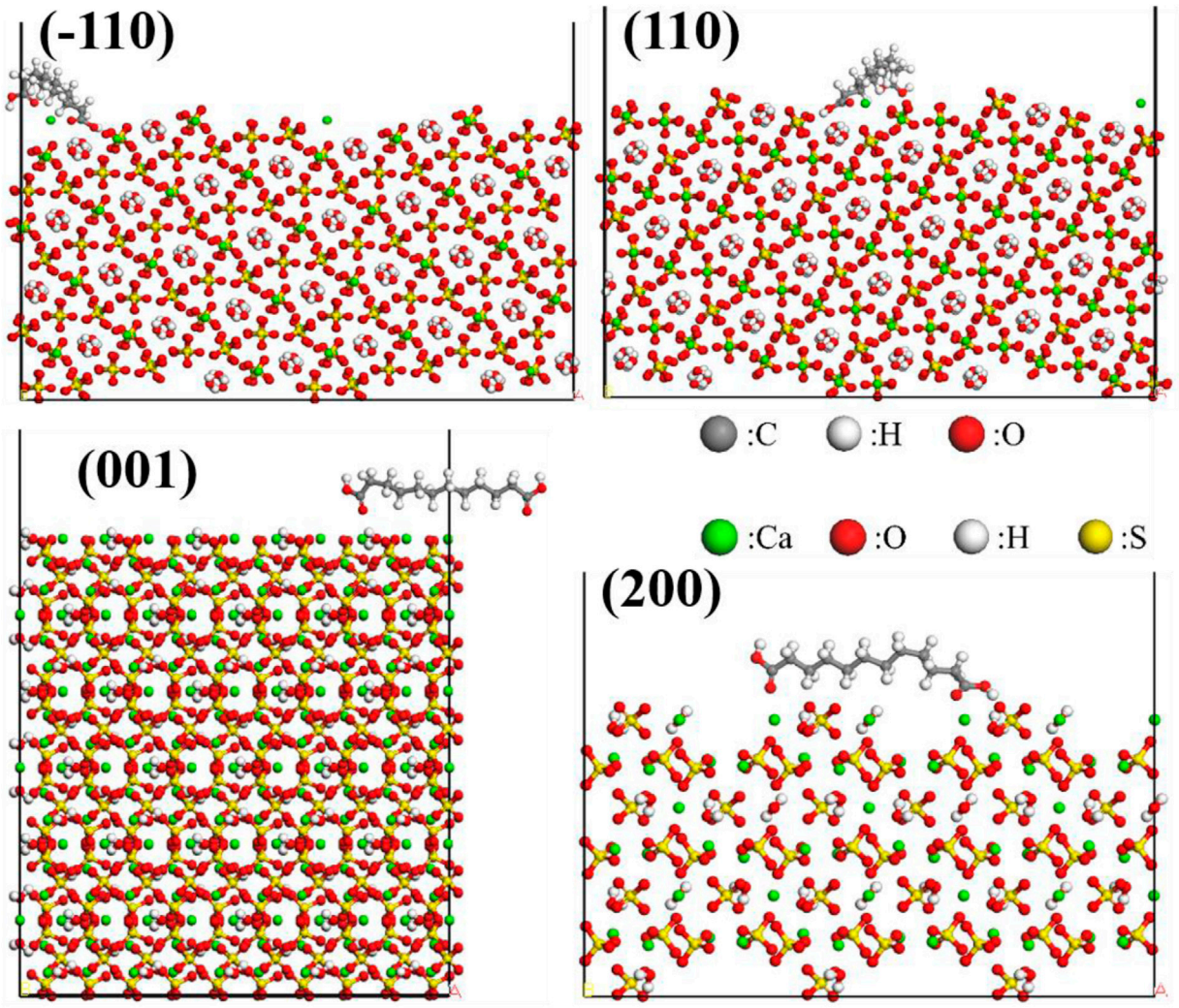

FIGURE 8
Adsorption models of dodecanedioic acid on the (001), (110), (–110), and (200) crystal planes of α-HH crystals obtained via molecular dynamics simulations.

These observations indicate that an appropriate spatial arrangement of carboxyl functional groups within the carboxylic acids is crucial for effective morphology control of α-HH crystals. This study identified an optimal range of 2–4 carbon atoms within the binary carboxylic acid molecular structure. Deviation from this range, in either direction, led to diminished crystal morphology control effects.

A positive correlation was observed between the number of carboxyl groups in the carboxylic acid modifier and the mechanical strength of α-HH. Specifically, α-HH modified with monocarboxylic acids exhibited significantly reduced mechanical strength compared to the reference sample. However, the presence of two carboxyl groups led to a substantial increase in mechanical strength, which continued to improve with three carboxyl groups. A further increase to four carboxyl groups resulted in only a marginal enhancement. These findings suggest that monocarboxylic acids do not exert a positive regulatory effect on α-HH crystal morphology. In contrast, binary and polycarboxylic acids exhibited a positive influence on α-HH crystal morphology, with the effect increasing alongside the number of carboxyl groups present. This influence plateaued slightly when the number of carboxyl groups reached three.

The presence of hydroxyl functional groups was found to contribute to the enhancement of α-HH mechanical strength. The influence of double carbon bonds on α-HH mechanical strength demonstrated a dependence on isomeric configuration. Specifically, cis-double carbon bonds led to an increase in mechanical strength, while trans-double carbon bonds resulted in a significant reduction. These findings suggest that the presence of hydroxyl groups and cis-double bonds exerts a positive regulatory influence on the α-HH crystal structure, whereas trans-double bonds do not exhibit such an effect.

The observed trends in mechanical strength can be attributed to the specific interactions between the carboxylic acid modifiers and the α-HH crystal surface. Modifiers with a suitable number and arrangement of carboxyl groups effectively interact with the crystal, influencing its growth habit and leading to enhanced mechanical properties. The presence of hydroxyl groups and cis-double bonds

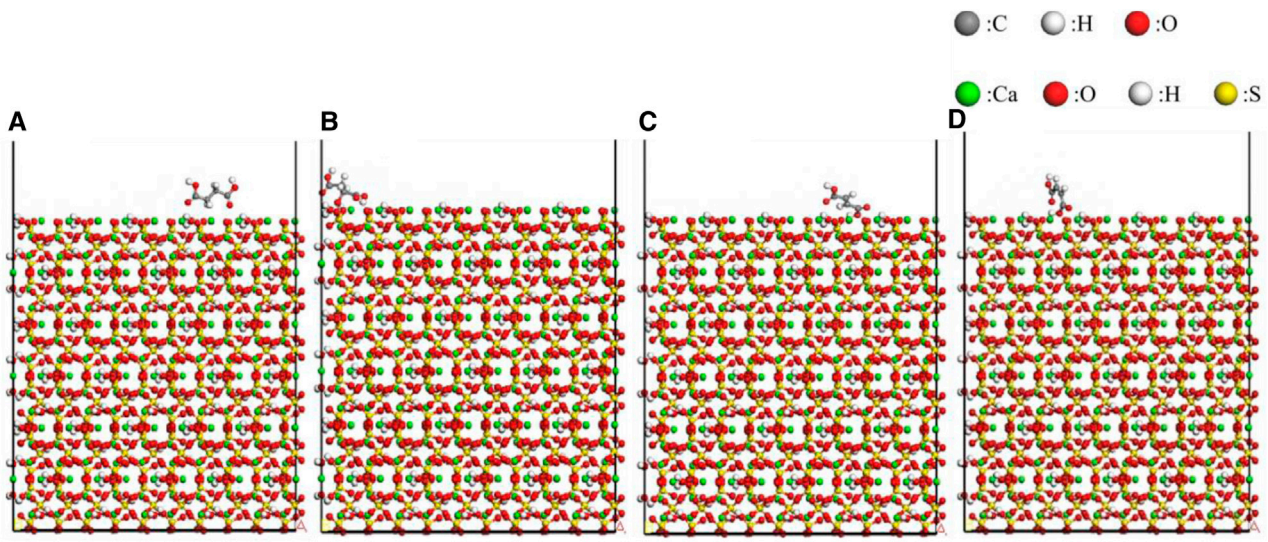

FIGURE 9
Adsorption models of different modifiers on (001) crystal plane of α-HH crystals obtained via molecular dynamics simulations: **(A)** succinic acid, **(B)** 2-hydroxy succinic aid, **(C)** reverse succinic aid, **(D)** maleic acid.

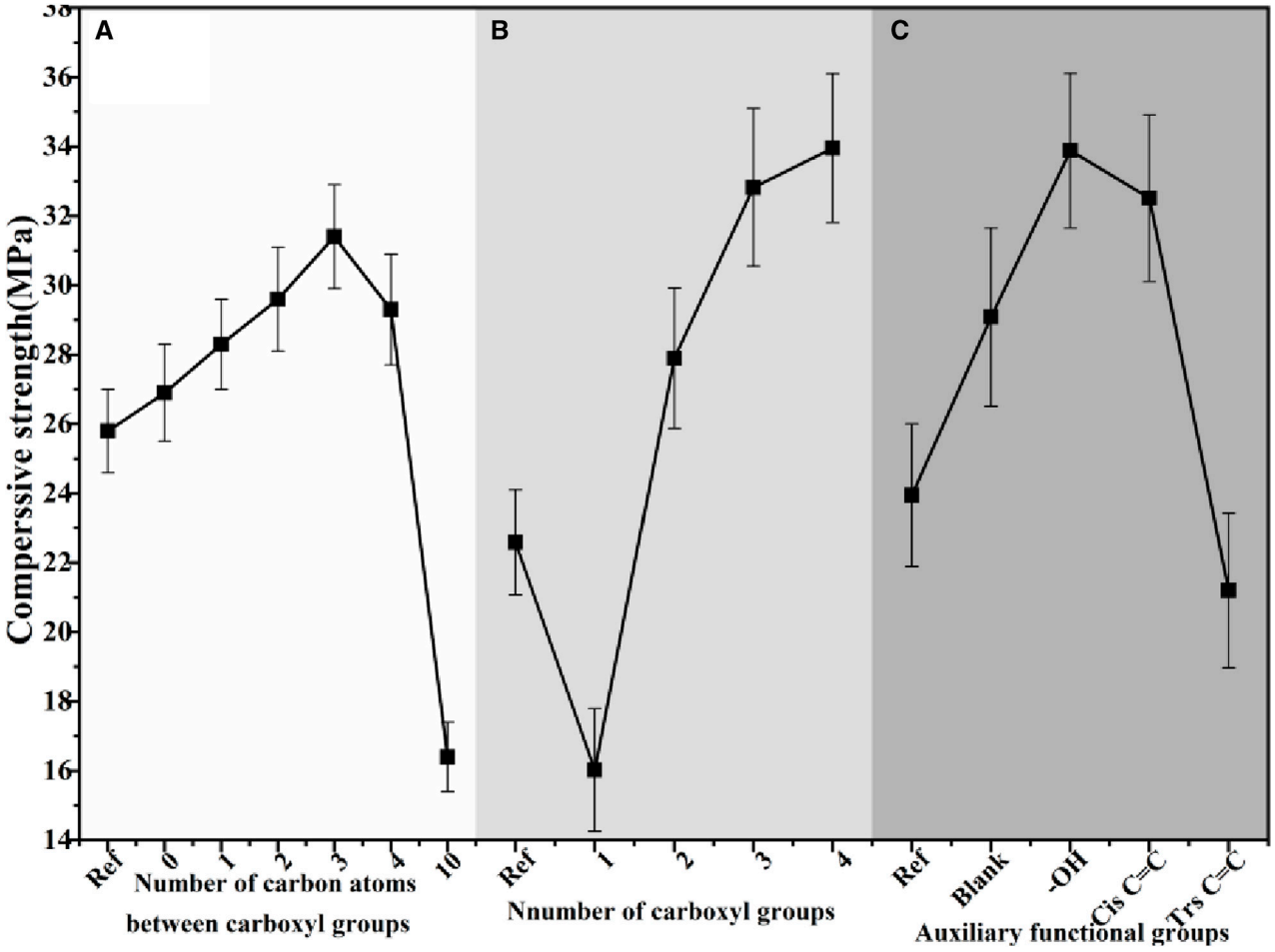

FIGURE 10
The compressive strength of α-HH samples prepared under the regulation of carboxylic acid modifier with different molecular structures: **(A)** carboxylic acid modifiers with varying numbers of carbon atoms in the carboxyl group interval, **(B)** carboxylic acid modifiers with varying numbers of carboxyl groups, **(C)** carboxylic acid modifiers with different auxiliary functional groups.

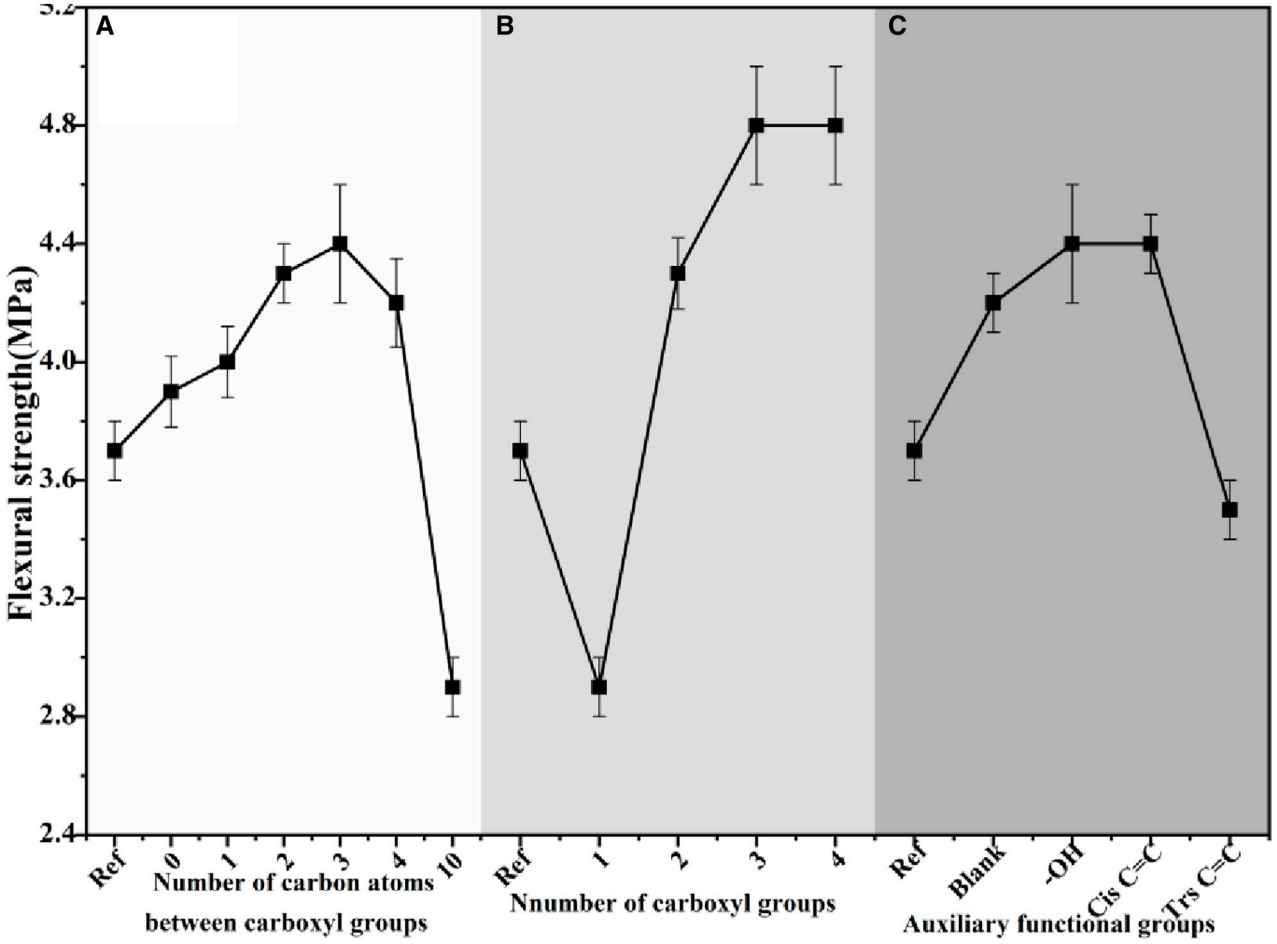

FIGURE 11
The flexural strength of α-HH samples prepared under the regulation of carboxylic acid modifier with different molecular structures:**(A)** carboxylic acid modifiers with varying numbers of carbon atoms in the carboxyl group interval, **(B)** carboxylic acid modifiers with varying numbers of carboxyl groups, **(C)** carboxylic acid modifiers with different auxiliary functional groups.

likely contributes to stronger interactions with the crystal surface, further promoting the formation of more robust structures.

4.2 Impact of modifiers on the micro-morphology of α-HH

Figure 12 presented SEM images of α-HH prepared with various carboxylic acid modifiers, highlighting the significant influence of modifier molecular structure on the resulting crystal morphology.

The number and arrangement of carboxyl groups within the modifier molecule significantly affected the α-HH crystal habit. As shown in Figures 12A–C, an increase in the number of carboxyl groups led to larger α-HH crystals with a decreased length-to-diameter ratio, resulting in a more complete crystal habit. This trend was evident when comparing blank α-HH (Figure 12A) to α-HH modified with succinic acid (Figure 12B) and EDTA (Figure 12C).

Further insights into the influence of functional groups were observed by comparing the effects of succinic acid (Figure 12B) and its derivatives. The addition of a hydroxyl group, as in 2-hydroxysuccinic acid (Figure 12F), enhanced the morphology control, yielding larger, shorter columnar crystals. Conversely, the incorporation of a trans-double carbon bond, as in reverse succinic acid (Figure 12D), significantly reduced crystal size while increasing the length-to-diameter ratio, resulting in elongated rod-like structures. In contrast, the presence of a cis-double carbon bond, as in maleic acid (Figure 12E), led to increased crystal size and a decreased aspect ratio, producing short columnar crystals.

The number of carbon atoms separating the carboxyl groups within the modifier molecule also influenced crystal morphology. An initial increase in α-HH crystal size followed by a decrease was observed as the number of spacer carbon atoms increased. With three spacer carbon atoms in glutaric acid (Figure 12G), α-HH crystals exhibited a reduced length-to-diameter ratio, resulting in short columnar crystals. When four spacer carbon atoms were present in adipic acid (Figure 12H), both crystal size and aspect ratio decreased, leading to a predominance of rod-shaped crystals. Finally, with ten spacer carbon atoms in dodecanedioic acid (Figure 12I), a significant reduction in crystal size and a transformation from rod-like to fiber-like morphology was observed.

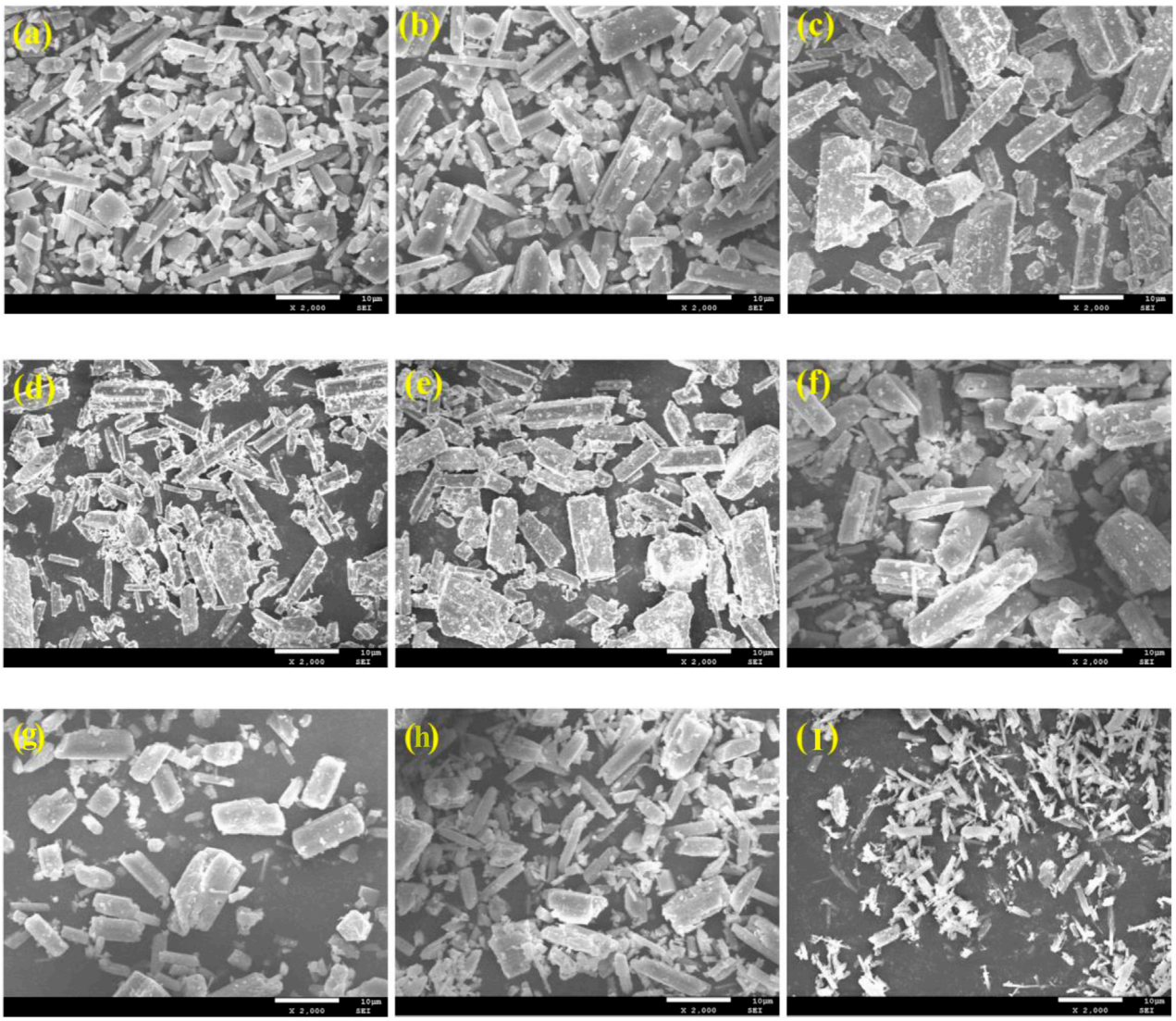

FIGURE 12
SEM images of α-HH prepared under the regulation of carboxylic acid modifier with different molecular structures: **(A)** blank, **(B)** succinic acid, **(C)** EDTA, **(D)** reverse succinic acid, **(E)** maleic acid, **(F)** 2-hydroxy succinic acid, **(G)** glutaric acid, **(H)** adipic acid, **(I)** dodecanedioic acid.

TABLE 2 Interaction energy of different carboxylic acid modifiers adsorbed on various crystal planes of α-HH crystal.

Modifiers	Interaction energy (ΔE)/(kcal/mol)			
	(001)	(110)	(-110)	(200)
Formic acid	−51.3 ± 2.4	−63.7 ± 2.7	−69.1 ± 3.1	−52.7 ± 2.0
Dodecanedioic acid	−107.6 ± 4.6	−122.5 ± 5.1	−127.7 ± 4.1	−108.4 ± 3.8

TABLE 3 Interaction energy of different carboxylic acid modifiers adsorbed on (001) crystal plane of α-HH crystal.

Modifiers	Interaction energy (ΔE)/(kcal/mol)
Succinic acid	−84.0 ± 2.4
2-hydroxy succinic acid	−98.4 ± 2.9
Reverse succinic acid	−74.8 ± 2.3
Maleic acid	−89.3 ± 2.7

4.3 Interaction energy between carboxylic acid modifiers and different α-HH crystal planes

Table 2 presents the interaction energies between the carboxylic acid modifiers and different α-HH crystal planes. Both formic acid and dodecanedioic acid exhibited higher adsorption energy values on the (110), (−110), and (200) crystal planes compared to the (001) plane. This indicated a preferential adsorption onto the lateral crystal planes, namely, (110), (−110), and (200), rather than the terminal (001) face of α-HH. Consequently, growth along the c-axis of the α-HH crystal is promoted, resulting in an increased aspect

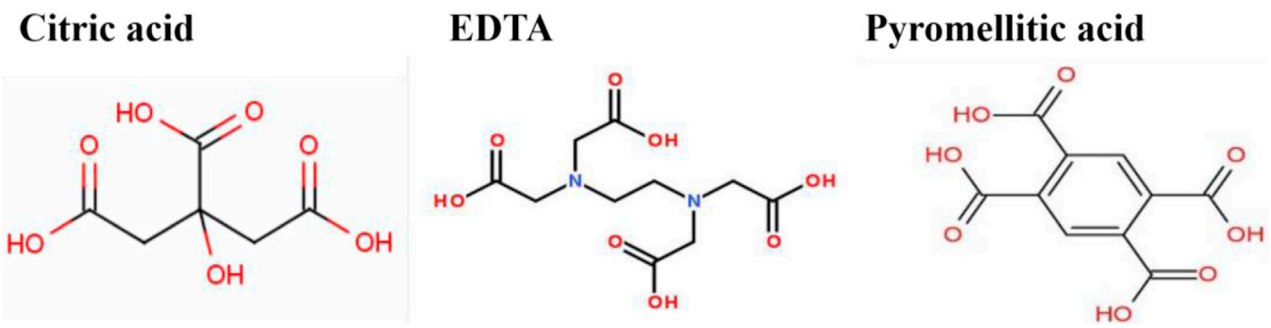

FIGURE 13
Molecular models of different carboxylic acid modifiers.

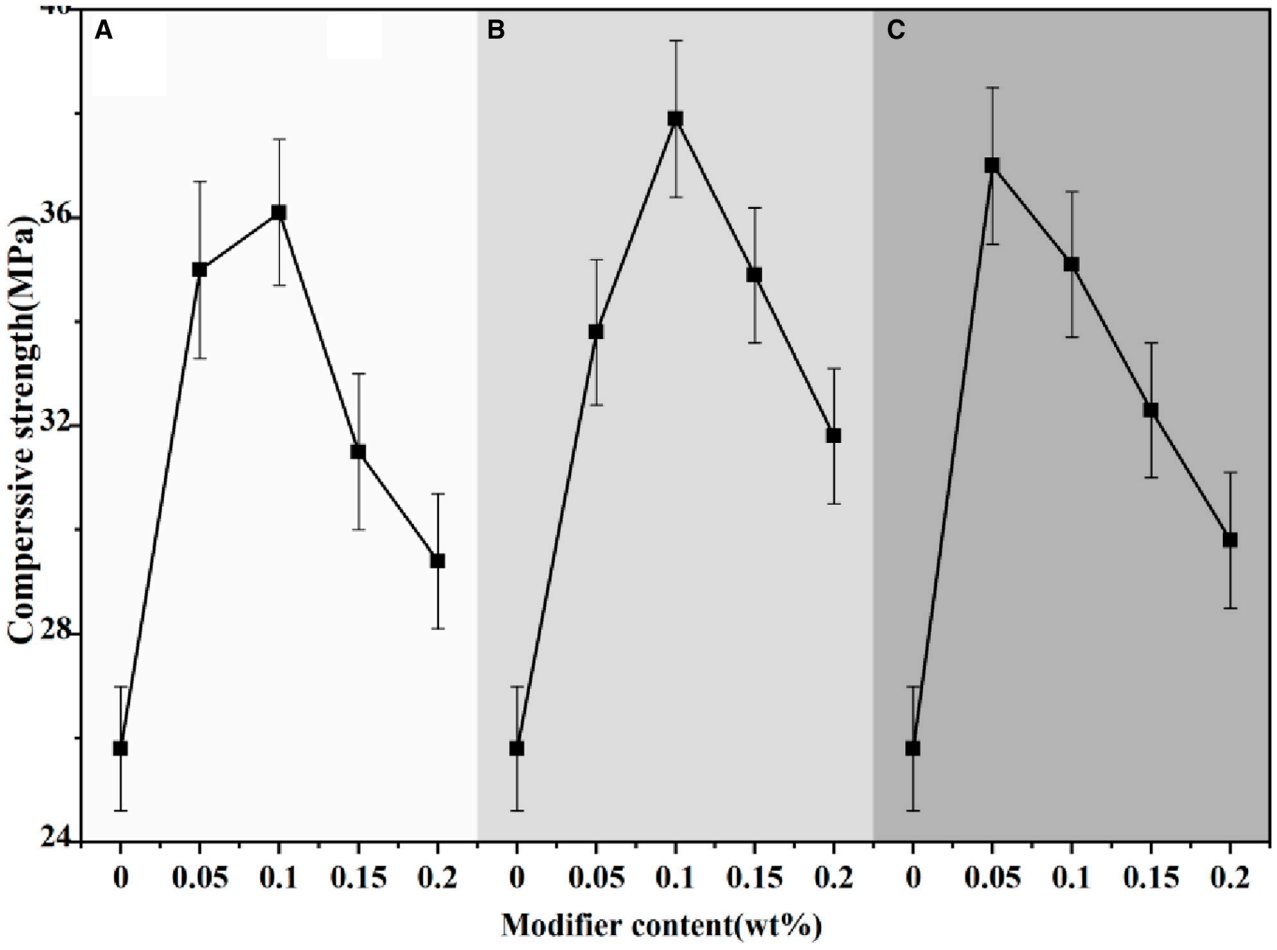

FIGURE 14
The compressive strength of α-HH with different modifier content (wt%):**(A)** Citric acid, **(B)** EDTA, **(C)** Pyromellitic acid.

ratio and a fibrous morphology. These simulation results were consistent with the experimental observations.

Table 3 displayed the interaction energy of different carboxylic acid modifiers adsorbed on the (001) crystal plane of α-HH. A comparative analysis revealed that both 2-hydroxysuccinic acid and maleic acid exhibited greater adsorption energies (in absolute values) than succinic acid on the (001) crystal plane, while the opposite was observed for fumaric acid (trans isomer of maleic acid). This suggests that the presence of hydroxyl groups and cis double carbon bonds within the carboxylic acid structure promotes adsorption onto the α-HH (001) surface, whereas trans double carbon bonds

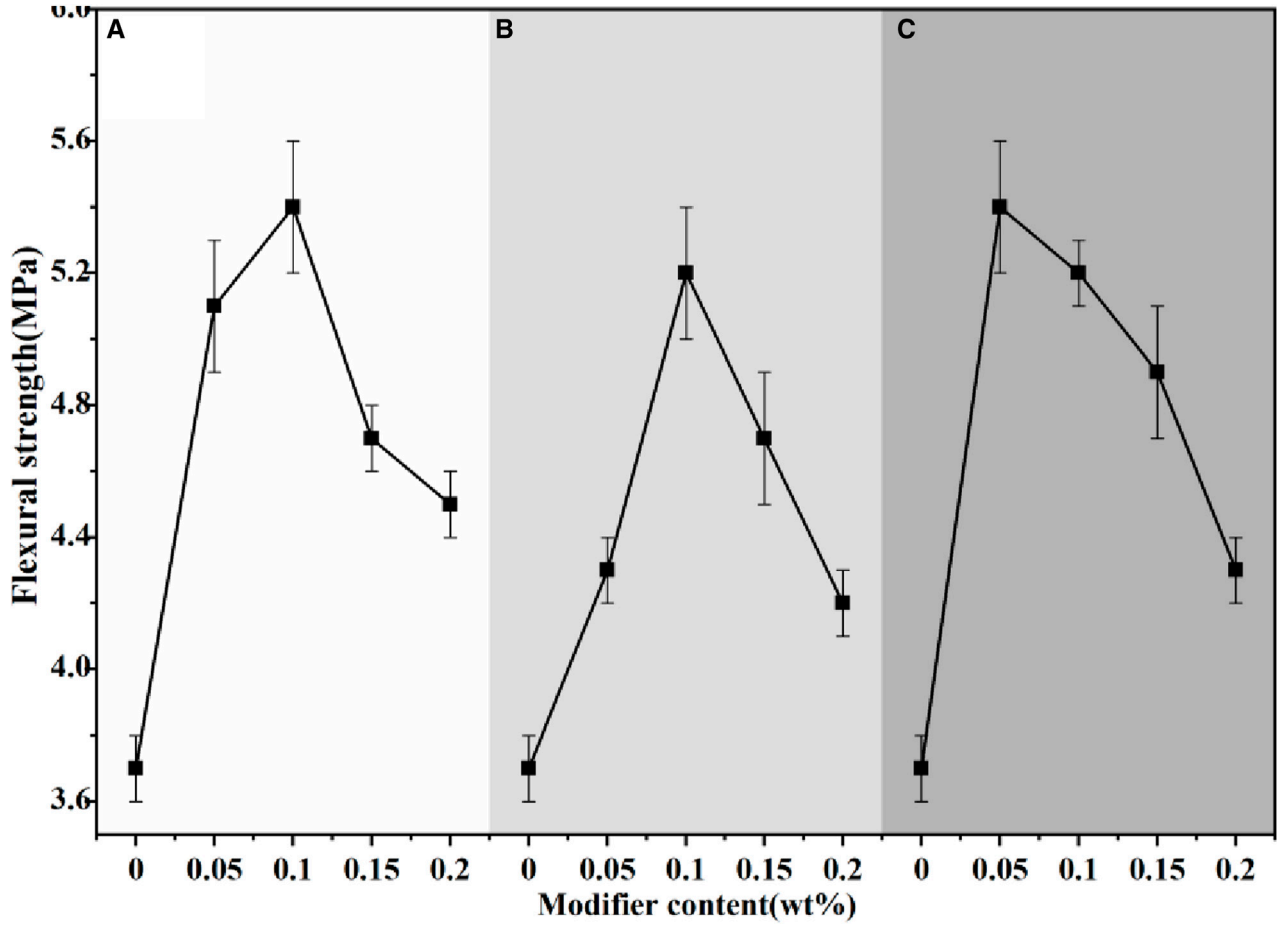

FIGURE 15
The flexural strength of α-HH with different modifier content (wt%): **(A)** Citric acid, **(B)** EDTA, **(C)** Pyromellitic acid.

hinder this process. Notably, among the investigated modifiers, 2-hydroxysuccinic acid demonstrated the strongest adsorption energy on the (001) crystal plane, followed by maleic acid. This finding indicates that hydroxyl groups exerted a more substantial influence on the adsorption behavior and, consequently, the crystal morphology of α-HH compared to cis double carbon bonds. Therefore, 2-hydroxysuccinic acid exhibited preferential adsorption onto the (001) crystal plane, leading to superior crystal morphology modification. These simulation results were corroborated by SEM observations.

4.4 Impact of citric acid, EDTA and pyromellitic acid on the mechanical strength and crystal morphology of α-HH

Building upon previous studies investigating the impact of carboxylic acid molecular structure on both the mechanical strength and crystal morphology of α-HH, citric acid, EDTA, and pyromellitic acid were identified as optimized modifiers for α-HH preparation. The molecular structures of these acids were depicted in Figure 13.

Figures 14, 15 depicted the mechanical strength of α-HH modified with various modifiers. Compared to the unmodified sample, the incorporation of modifiers led to a significant improvement in mechanical strength. For citric acid and EDTA, the observed trend was an initial increase in strength with increasing additive content, followed by a subsequent decrease. In contrast, the strength gradually declined as the content of pyromellitic acid increased. To achieve a compressive strength of 35 MPa in α-HH, the optimal content ranges were 0.05%–0.10% for citric acid, 0.10%–0.15% for EDTA, and 0.05%–0.10% for pyromellitic acid.

Figure 16 and Table 4 demonstrated the significant impact of different modifiers on the morphology and size distribution of α-HH crystals. The aspect ratio of the α-HH crystals was determined by measuring the length and width of at least 50 individual particles in ImageJ software. Unmodified α-HH crystals exhibited a distinct elongated rod-like morphology with a high aspect ratio of approximately 9:1. This indicated a pronounced anisotropic growth along a specific crystallographic axis. The blank sample displayed a relatively narrow size distribution, with an average length of 10.4 μm and an average width of 1.2 μm. This suggested a relatively

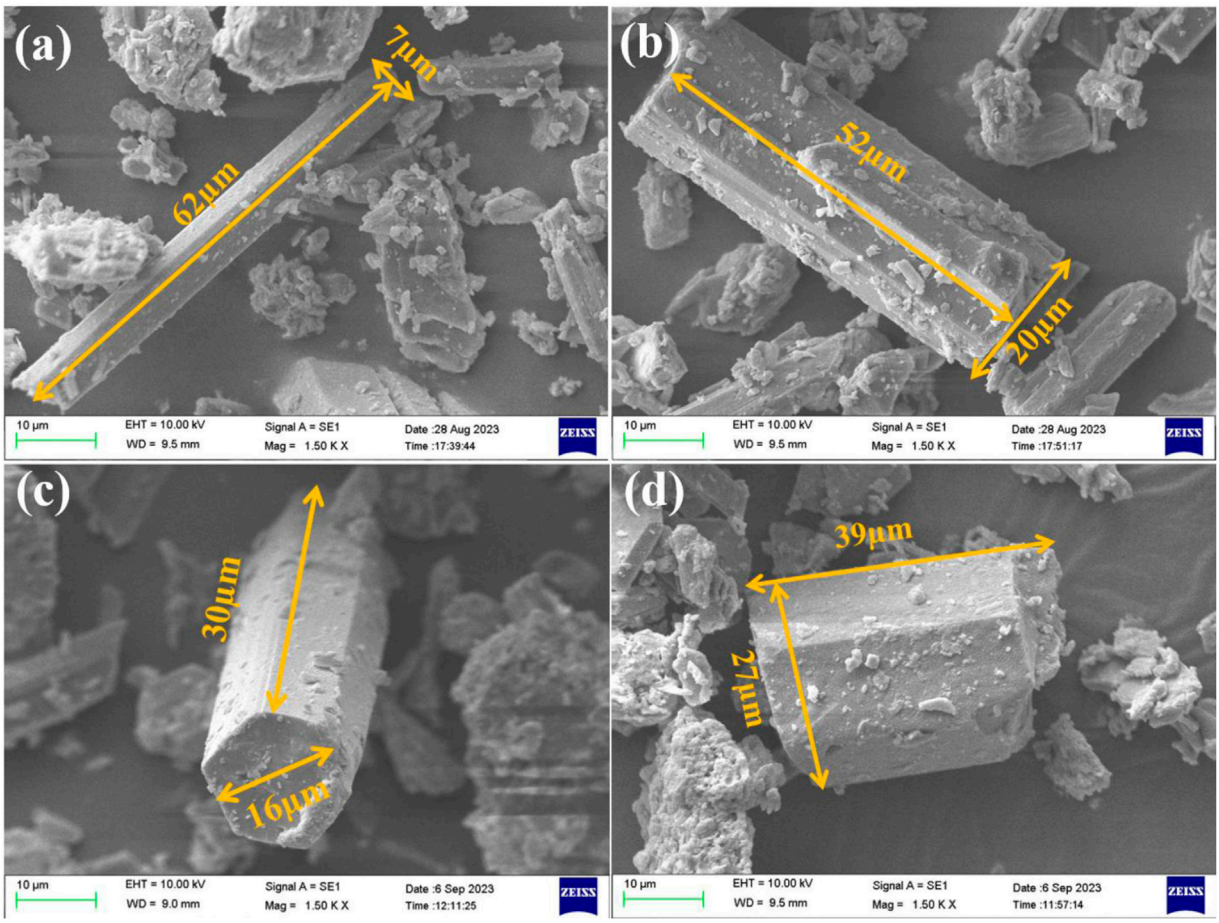

FIGURE 16
The SEM images of α-HH with different modifiers:**(A)** blank sample, **(B)** 0.1%citric acid, **(C)** 0.1%EDTA, **(D)** 0.05% pyromellitic acid.

TABLE 4 Average size and aspect ratio of α-HH crystals with different modifiers.

Modifier	Average length (μm)	Standard deviation (μm)	Average width (μm)	Standard deviation (μm)	Aspect ratio	Standard deviation
Blank	10.4	1.6	1.2	0.2	9.1	1.2
Citric acid	17.2	2.4	4.4	0.6	4.2	0.8
EDTA	21.2	3	6	0.7	3.5	0.7
Pyromellitic acid	6	0.9	4	0.6	1.5	0.2

consistent growth process for the unmodified crystals. Citric acid modification significantly altered the morphology of α-HH crystals, leading to a reduction in aspect ratio to 4.2:1. The crystals became shorter and wider, taking on a more columnar shape. The average length increased to 17.2 μm, while the average width increased to 4.4 μm. However, the size distribution appeared to be slightly broader than the blank sample. The presence of smaller particles (as observed in Figure 16B) might explain this. EDTA modification led to the formation of crystals with smooth surfaces and well-defined hexagonal end faces. This indicated that EDTA influenced the crystal growth process, promoting the formation of more regular and symmetric structures. The average length increased further to 21.2 μm, and the average width to 6.0 μm. The aspect ratio slightly decreased to 3.5:1, indicating a further reduction in length-to-width ratio compared to the blank sample. The size distribution remained relatively narrow, suggesting a controlled growth process with EDTA. Pyromellitic acid modification had a significant impact on crystal morphology, drastically decreasing the aspect ratio to 1.5:1.

The crystals became very short and wide, appearing almost cube-like. This indicated a strong influence on the anisotropic growth, leading to more uniform growth along all axes. The average length decreased to 6.0 μm, while the average width was 4.0 μm. The size distribution was relatively narrow, indicating a consistent growth process even with this drastic change in morphology.

The results demonstrated that the introduction of different modifiers significantly affected the morphology and size distribution of α-HH crystals. The modifiers can influence the crystal growth kinetics, altering the relative rates of growth along different crystallographic axes.

5 Conclusion

This study investigated the impact of carboxylic acid modifiers on the crystal morphology and mechanical properties of α-HH. The findings highlight the significant role of the number, arrangement, and type of functional groups within the modifier structure in regulating crystal growth.

(1) The number and arrangement of carboxyl groups within the modifier significantly influenced the crystal morphology. Dicarboxylic acids with 2–4 inter-carboxyl carbons demonstrated the most effective regulatory ability. Modifiers with a single carboxyl group or a wider separation between carboxyl groups (e.g., 10 carbons) promoted elongation by preferentially adsorbing to the side faces of the crystal. Conversely, hydroxyl or cis-double carbon bond substitutions favored adsorption on the (001) plane, leading to shorter crystals. Trans-double carbon bonds showed negligible effects on crystal morphology.
(2) The adsorption energy of carboxylic acid modifiers on different crystal planes of α-HH varied significantly. Succinic acid, 2-hydroxy succinic acid, reverse succinic acid, and maleic acid exhibited distinct adsorption energies on the (001) plane. Additionally, the adsorption energies of formic acid and dodecanedioic acid differed across various crystal planes, suggesting their preferential adsorption to specific crystallographic orientations.
(3) Citric acid, EDTA, and pyromellitic acid emerged as highly effective modifiers for α-HH, facilitating the transformation of fine-rod crystals into short columnar structures. Optimal concentrations of these modifiers were found to be 0.05%–0.10% for citric acid, 0.10%–0.15% for EDTA, and 0.05%–0.10% for pyromellitic acid. At these concentrations, α-HH exhibited enhanced mechanical properties, with flexural strengths exceeding 4 MPa and compressive strengths greater than 35 MPa.

In summary, this study demonstrates the crucial role of carboxylic acid modifiers in controlling α-HH crystal morphology and mechanical properties. By understanding the structure-activity relationships of these modifiers and their adsorption behavior on specific crystal planes, it is possible to effectively tailor the crystal growth process to achieve desired properties for α-HH applications. Future research could further explore the impact of other functional groups and molecular structures on α-HH crystal morphology and investigate the potential of these modifiers for enhancing other material properties.

Data availability statement

The original contributions presented in the study are included in the article/Supplementary Material, further inquiries can be directed to the corresponding author.

Author contributions

G-gL: Formal Analysis, Investigation, Methodology, Validation, Writing–original draft. J-eL: Validation, Writing–review and editing. LM: Investigation, Methodology, Writing–review and editing. H-lG: Supervision, Writing–review and editing. S-hY: Conceptualization, Supervision, Validation, Writing–review and editing.

Funding

The author(s) declare that financial support was received for the research, authorship, and/or publication of this article. The authors gratefully acknowledge the financial support from ministry of housing and urban-rural development of China (No. 2021K064) and the ministry of industry and information technology of China (No. KF22028).

Conflict of interest

Authors G-gL and J-eL were employed by Hubei Yuangu New Building Materials Technology Co., LTD.

The remaining authors declare that the research was conducted in the absence of any commercial or financial relationships that could be construed as a potential conflict of interest.

Publisher's note

References

1. Vásconez-Maza MD, Bueso MC, Mulas J, Faz Á, Martínez-Segura MA. Characterising an abandoned phosphogypsum deposit by combining radiological, geophysical, geochemical, and statistical techniques. *CATENA* (2022) 216:106401. doi:10.1016/j.catena.2022.106401

2. Cui R, Bai H, Gao Y, Xiu X. Current situation of comprehensive utilization of phosphor gypsum and development trend of "14th Five-Year Plan". *Inorg salt industry* (2022) 54(4):1–4. doi:10.19964/j.issn.1006-4990.2022-0086

3. Yang R, et al. The "14th Five-Year Plan" strategy of "three phosphorus" comprehensive remediation in the Yangtze River Basin. *Ecol Economy* (2021) 37(3): 187–91.

4. Xu J, et al. Research status of environmental impact under the background of comprehensive utilization of phosphogypsum. *J Mining Sci* (2023) 8(1):115–26. doi:10.19606/j.cnki.jmst.2023.01.011

5. Pliaka M, Gaidajis G. Examination of the environmental behavior of phosphogypsum with the application of lab-scale experiment. *J Environ Scienceand Health,A* (2023) 58(7):706–14. doi:10.1080/10934529.2023.2208994

6. Zhao Y, et al. Pollution of "three phosphorus" in the Yangtze River basin and countermeasures. *Environ Impact Assess* (2020) 42(6):1–5. doi:10.14068/j.ceia.2020.06.001

7. Zhao B, Wang G, Zhao K, Wang M, Wu B, Li S, et al. Mechanical properties, permeability and microstructure of steam-cured fly ash mortar mixed with phosphogypsum. *Construction Building Mater* (2023) 400:132582. doi:10.1016/j.conbuildmat.2023.132582

8. Zhang L, Mo KH, Yap SP, Gencel O, Ling TC. Mechanical strength, water resistance and drying shrinkage of lightweight hemihydrate phosphogypsum-cement composite with ground granulated blast furnace slag and recycled waste glass. *Construction Building Mater* (2022) 345:128232. doi:10.1016/j.conbuildmat.2022.128232

9. Wang Y, Huo H, Chen B, Cui Q. Development and optimization of phosphogypsum-based geopolymer cement. *Construction Building Mater* (2023) 369: 130577. doi:10.1016/j.conbuildmat.2023.130577

10. Sun T, Li W, Xu F, Yu Z, Wang Z, Ouyang G, et al. A new eco-friendly concrete made of high content phosphogypsum based aggregates and binder: mechanical properties and environmental benefits. *J Clean Prod* (2023) 400:136555. doi:10.1016/j.jclepro.2023.136555

11. Dong Z, et al. Research progress on resource utilization of phosphor gypsum building materials. *Inorg Salt Industry* (2022) 54(4):5–9. doi:10.19964/j.issn.1006-4990.2021-0346

12. Du M, Wang J, Dong F, Wang Z, Yang F, Tan H, et al. The study on the effect of flotation purification on the performance of α-hemihydrate gypsum prepared from phosphogypsum. *Scientific Rep* (2022) 12(1):95. doi:10.1038/s41598-021-04122-w

13. Fornes IV, Vaičiukynienė D, Nizevičienė D, Doroševas V, Michalik B. A. comparative assessment of the suitability of phosphogypsum from different origins to be utilised as the binding material of construction products. *J Building Eng* (2012) 44: 102995. doi:10.1016/j.jobe.2021.102995

14. Garg M, Jain N, Singh M. Development of alpha plaster from phosphogypsum for cementitious binders. *Construction Building Mater* (2009) 23(10):3138–43. doi:10.1016/j.conbuildmat.2009.06.024

15. Xiao YD, Jin HX, Wang ML, Guo YL. Collaborative utilization status of red mud and phosphogypsum: a review. *J Sustain Metall* (2022) 8(4):1422–34. doi:10.1007/s40831-022-00569-x

16. Thakur Y, Tyagi A, Sarkar S. Utilization of industrial waste phosphogypsum as geomaterial: a review. *J Hazard Tox Radioactive Waste* (2023) 27(2):03123001. doi:10.1061/JHTRBP.HZENG-1181

17. Cichy B, et al. Geotechnical properties of phosphogypsum and its use in road engineering. In: Proceedings of China-Europe Conference on Geotechnical Engineering. Cham: Springer International Publishing (2018). p. 1664–7. doi:10.1007/978-3-319-97115-5_166

18. Zhou Y, Li X, Shi Y, Zhu Q, Du J. Reuse of phosphogypsum pretreated with water washing as aggregate for cemented backfill. *Scientific Rep* (2022) 12(1):16091. doi:10.1038/s41598-022-20318-0

19. Ma B, Lu W, Li Y, Gao C, He X. Synthesis of α-hemihydrate gypsum from cleaner phosphogypsum. *J Clean Prod* (2018) 195:396–405. doi:10.1016/j.jclepro.2018.05.228

20. Chen L, Yang L, Cao J. Utilization of phosphogypsum to synthesize α-hemihydrate gypsum in H_3PO_4–H_2O solution. *Construction Building Mater* (2023) 368:130453. doi:10.1016/j.conbuildmat.2023.130453

21. Jin Z, Cui C, Xu Z, Lu W, He X, et al. Recycling of waste gypsum from αlpha-hemihydrate phosphogypsum: based on the atmospheric hydrothermal process. *Construction Building Mater* (2023) 377:131136. doi:10.1016/j.conbuildmat.2023.131136

22. Liu S, Asselin E, Li Z. Preparation of α-high-strength hemihydrate from flue gas desulfurization gypsum in $AlCl_3$ -$MgCl_2$ solution at atmospheric pressure. *Ind Eng Chem Res* (2022) 61(37):14110–20. doi:10.1021/acs.iecr.2c02280

23. Fang Z, Gao W, Ai H, Pei M, Guo W, Wang L. Effect of polyaspartic acid on the setting time and mechanical properties of α-hemihydrate gypsum. *Construction Building Mater* (2023) 373:130894. doi:10.1016/j.conbuildmat.2023.130894

24. Mi Y, Chen D, He Y, Wang S. Morphology-controlled preparation of α-calcium sulfate hemihydrate from phosphogypsum by semi-liquid method. *Cryst Res Technol* (2018) 53(1):1700162. doi:10.1002/crat.201700162

25. Shao D, Zhao B, Zhang H, Wang Z, Shi C, Cao J. Preparation of large-grained α-high strength gypsum with FGD gypsum. *Cryst Res Technol* (2017) 52(7):1700078. doi:10.1002/crat.201700078

26. Xie Y, Yang L, Wang C, Feng X, Tang Z, Liu Z. Production and properties of the polyvinyl alcohol modified macro-defect-free α-hemihydrate gypsum composite. *Construction Building Mater* (2023) 375:130721. doi:10.1016/j.conbuildmat.2023.130721

27. Taher R, et al. Carboxylic acids: effective inhibitors for calcium sulfate precipitation. *Mineralogical Mag* (2014) 78(6):1465–72. doi:10.1180/minmag.2014.078.6.13

28. Polat S, Sayan P. Determination of the effects of carboxylic acids on calcium sulfate dihydrate crystallization. *Chem Eng Technol* (2017) 40(7):1354–61. doi:10.1002/ceat.201600525

29. Polat S, Sayan P. Effects of tricarballylic acid on phase transformation of calcium sulfate hemihydrate to the dihydrate form. *Cryst.Res.Technol.* (2017) 52(5):1600395. doi:10.1002/crat.201600395

30. Duan Z, Li J, Li T, Zheng S, Han W, Geng Q, et al. Influence of crystal modifier on the preparation of α-hemihydrate gypsum from phosphogypsum. *Construction Building Mater* (2017) 133:323–9. doi:10.1016/j.conbuildmat.2016.12.060

31. Guan Q, Sun W, Hu Y, Yin Z, Zhang C, Guan C, et al. Simultaneous control of particle size and morphology of α-Ca SO_4·1/2H_2O with organic additives. *J Am Ceram Soc* (2019) 102(5):2440–50. doi:10.1111/jace.16177

32. Follner S, Wolter A, Preusser A, Indris S, Silber C, Follner H. The setting behaviour of α- and β-$CaSO_4$·0.5H_2O as a function of crystal structure and morphology. *Cryst Res Technol* (2022) 37(10):1075–87. doi:10.1002/1521-4079(200210)37:10<1075::aid-crat1075>3.0.co;2-x

33. Zhang J, Wang X, Hou P, Jin B, Zhang X, Li Z. Effect of phosphoric acid on the preparation of α-hemihydrate gypsum using hydrothermal method. *Materials* (2023) 16(17):5878. doi:10.3390/ma16175878

34. Zhang J, et al. Research progress on comprehensive utilization of phosphor gypsum materials. *Mater Rev* (2023) 37(16):167–78.

35. China Building Materials Industry Standardization Institute. *Test methods for physical properties of ordinary gypsum plaster (*JC/T*2038–2010)* (2010).

36. Bezou C, Nonat A, Mutin JC, Christensen A, Lehmann M. Investigation of the crystal structure of γ-$CaSO_4$, $CaSO_4$·0.5H_2O, and $CaSO_4$·0.6H_2O by powder diffraction methods. *Solid State Chem* (1995) 117:165–76. doi:10.1006/jssc.1995.1260

37. Tang YB, Gao J. Investigation of the effects of sodium dicarboxylates on the crystal habit of calcium sulfate α-hemihydrate. *Langmuir* (2017) 33(38):9637–44. doi:10.1021/acs.langmuir.7b02380

38. Wang L-J, Liu G-S, Song X-F, Yu J-G. Molecular modeling for selective adsorption of halite with dodecylmorpholine. *Acta Phys* (2009) 25(5):963–9. doi:10.3866/PKU.WHXB20090424